Three-Dimensional Personalized Monte Carlo Dosimetry in ^{90}Y Resin Microspheres Therapy of Hepatic Metastases: Nontumoral Liver and Lungs Radiation Protection Considerations and Treatment Planning Optimization

Alice Petitguillaume[1], Michela Bernardini[2], Lama Hadid[1], Claire de Labriolle-Vaylet[3,4], Didier Franck[1], and Aurélie Desbrée[1]

[1]Laboratoire d'Evaluation de la Dose Interne (LEDI), Institut de Radioprotection et de Sûreté Nucléaire (IRSN), Fontenay-Aux-Roses, France; [2]Nuclear Medicine Department, Hôpital Européen Georges Pompidou (HEGP), Paris, France; [3]UPMC, Univ Paris 06 Biophysics, Paris, France; and [4]Nuclear Medicine Department, Hôpital Trousseau, Paris, France

In the last decades, selective internal radiation therapy (SIRT) has become a real alternative in the treatment of unresectable hepatic cancers. In practice, the activity prescription is limited by the irradiation of organs at risk (OAR), such as the lungs and nontumoral liver (NTL). Its clinical implementation is therefore highly dependent on dosimetry. In that context, a 3-dimensional personalized dosimetry technique—personalized Monte Carlo dosimetry (PMCD)—based on patient-specific data and Monte Carlo calculations was developed and evaluated retrospectively on clinical data. **Methods:** The PMCD method was evaluated with data from technetium human albumin macroaggregates (^{99m}Tc-MAA) evaluations of 10 patients treated for hepatic metastases. Region-of-interest outlines were drawn on CT images to create patient-specific voxel phantoms using the OEDIPE software. Normalized 3-dimensional matrices of cumulated activity were generated from ^{99m}Tc-SPECT data. Absorbed doses at the voxel scale were then obtained with the MCNPX Monte Carlo code. The maximum-injectable activity (MIA) for tolerance criteria based on either OAR mean absorbed doses (D_{mean}) or OAR dose-volume histograms (DVHs) was determined using OEDIPE. Those MIAs were compared with the one recommended by the partition model (PM) with D_{mean} tolerance criteria. Finally, OEDIPE was used to evaluate the absorbed doses delivered if those activities were injected to the patient and to generate the corresponding isodose curves and DVHs. **Results:** The MIA recommended using D_{mean} tolerance criteria is, in average, 27% higher with the PMCD method than with the PM. If tolerance criteria based on DVHs are used along with the PMCD, an increase of at least 40% of the MIA is conceivable, compared with the PM. For MIAs calculated with the PMCD, D_{mean} delivered to tumoral liver (TL) ranged from 19.5 to 118 Gy for D_{mean} tolerance criteria whereas they ranged from 26.6 to 918 Gy with DVH tolerance criteria. Thus, using the PMCD method, which accounts for fixation heterogeneities, higher doses can be delivered to TL. Finally, absorbed doses to the lungs are not the limiting criterion for activity prescription. However, D_{mean} to the lungs can reach 15.0 Gy. **Conclusion:** Besides its feasibility and applicability in clinical routine, the interest for treatment optimization of a personalized Monte Carlo dosimetry in the context of SIRT was confirmed in this study.

Key Words: Monte Carlo dosimetry; OEDIPE; dose-volume histograms; SIRT; hepatic metastases

J Nucl Med 2014; 55:405–413
DOI: 10.2967/jnumed.113.120444

Liver cancer is the third most common cause of death from cancer worldwide (*1*), the most frequent type being hepatocellular carcinoma (HCC). Notably, because the hepatic portal vein conveys blood from the gastrointestinal tract to the liver, this organ is also the most common place for metastases development. Indeed, around 50% of patients with colorectal cancer will develop liver metastases (*2*) and the median survival of those patients is the same whether the primary cancer is treated or not. Liver metastases are therefore the predominant prognostic factor, which makes their treatment essential. Among the conceivable therapies, surgical resection or liver transplantation are the most effective for both HCC and liver metastases. However, in western countries, less than 20% of patients with liver cancer may benefit from surgical resection (*3,4*).

Selective internal radiation therapy (SIRT) was introduced in clinical practice in the 1990s in Australia as an alternative in the treatment of unresectable hepatic tumors (*5*). This therapy, also called radioembolization, consists of the injection of microspheres labeled with ^{90}Y into the lesions via the hepatic artery. Thanks to the vascular specificities of the liver and the tumoral lesions, those microspheres are trapped preferentially in the tumoral tissue capillaries. However, the surrounding tissues can be significantly irradiated. Thus, to ensure both the patient's radiation protection and therapy optimization, accurate treatment planning must be performed. To achieve that aim, evaluations requiring several steps are carried out. First, a high-resolution CT scan is acquired. Vascular angiography is then performed to obtain a precise cartography of the liver and the lesion vascular beds. If required, prophylactic embolizations might be used to enhance the therapy selectivity and to prevent microsphere fixations in unwanted locations. SPECT/CT is finally performed after the injection of technetium human albumin macroaggregates (^{99m}Tc-MAA; Pulmocis;

Received Jan. 23, 2013; revision accepted Sep. 18, 2013.
For correspondence or reprints contact: Aurélie Desbrée, Institut de Radioprotection et de Sûreté Nucléaire, PRP-HOM/SDI/LEDI, 31, avenue de la Division Leclerc, 92 260 Fontenay-Aux-Roses, France.
E-mail: aurelie.desbree@irsn.fr
Published online Feb. 6, 2014.

Cisbio International), which are supposed to mimic the future distribution of microspheres.

The maximum activity to be injected to the patient is then determined using one of the following conventional methods: the body surface area method (*6*) or the partition model (PM) (*7,8*). The body surface area method is an empiric approach in which injected activity is adjusted depending on tumor burden (TB) and the patient's physical characteristics. The PM is based on the MIRD approach in which limit values on mean absorbed doses (D_{mean}) to organs at risk (OAR), that is, the lungs and nontumoral liver (NTL), are considered. Although it accounts more realistically for the therapy selectivity, the main drawback of the PM is the underlying assumption of homogeneous activity distributions within the regions of interest (ROI). Furthermore, conventional methods cannot provide dose-volume histograms (DVHs) that have been shown as extremely valuable for the assessment of tumor control probability and normal tissue toxicity (*9*).

Recent studies have proposed the development of 3-dimensional (3D) dosimetry based on voxel dose kernel convolution for patients treated for HCC (*10,11*). The main limitation of this approach is that it does not account for tissue density nonuniformities and, thus, for their impact on absorbed dose calculations at the liver boundaries, in particular at the interface between lungs and soft tissues.

The use of Monte Carlo methods to simulate radiation transport has become the most accurate means to predict absorbed dose distributions and derive quantities of interest for the radiation treatment of cancer patients (*12*). Some software, dedicated to patient-specific Monte Carlo simulations and based on robust electron transport code, is increasingly called upon to be used in clinical practice (*13–15*). In this context, in collaboration with the Hôpital Européen Georges Pompidou (HEGP, Paris, France), the OEDIPE software (*14,16*) associated with the MCNPX Monte Carlo code (*17*) was used in a retrospective study of treatment-planning methods in SIRT. Data from 10 patients treated for hepatic metastases using ^{90}Y resin microspheres were collected. Patient-specific Monte Carlo dosimetry (PMCD) was retrospectively performed at the voxel scale from ^{99m}Tc-MAA SPECT data, which describe the activity distribution heterogeneity. The maximum-injectable activity (MIA) was determined according to OAR tolerance criteria based on 2 different references: D_{mean} and DVHs. The results were compared with the MIA calculated using the PM. D_{mean} to NTL and tumoral liver (TL), isodose curves, and DVHs were assessed depending on the MIAs. Taking advantage of Monte Carlo calculation possibilities, dosimetry to the lungs was also achieved. Finally, a study on computation time and associated uncertainties was carried out.

MATERIALS AND METHODS

Patient Studies

After signing an informed consent form, patients were treated at HEGP following an established course of treatment approved by the institutional review board. This predosimetry study was performed retrospectively using data, already available, for 10 patients treated for hepatic metastases from colorectal and endocrine cancers. Data from a high-resolution CT scan of the thorax–abdomen region, acquired for diagnosis, were collected for each patient to get anatomic information. Six patients underwent a single ^{99m}Tc-MAA evaluation before treatment, and 4 patients underwent 2 evaluations successively with or without additional prophylactic embolizations. Depending on the therapeutic strategy, these injections were performed either in the whole liver or in 1 lobe and were followed, 15 d after the last evaluation, by SIRT using SIR-Spheres microspheres (Sirtex Medical Limited) (*6*). For these 14 evaluations, data from ^{99m}Tc whole-body scintigraphy and ^{99m}Tc SPECT/CT of the abdomen were collected to assess the activity distribution in the lungs, liver, and abdomen. These examinations were acquired within 1 h after the ^{99m}Tc-MAA injection on an Infinia-Hawkeye hybrid γ camera (GE Healthcare) equipped with a standard low-energy high-resolution collimator. SPECT imaging was performed with an energy window at 140 keV $\pm$ 10% and 60 frames of 30 s in a 128 $\times$ 128 matrix. The CT scan (120 kV, 2.5 mA) was acquired in axial mode with a 5-mm slice thickness. SPECT was reconstructed using an ordered-subset expectation maximization algorithm with 10 subsets and 3 iterations, Butterworth (0.44,10) prefiltering, Hann (1.56) postfiltering, and CT-based attenuation correction.

PMCD General Principles

Patient-Specific Voxel Phantoms. TL, NTL, right lung, left lung, and remaining tissues (RT) were semiautomatically segmented on the patient CT scan using the imaging module IMAgo of Isogray software (Dosisoft). TL and NTL were segmented considering the whole liver for all types of treatments. ROI delineations were then imported into the OEDIPE software, developed at Institut de radioprotection et de Sûreté Nucléaire (IRSN, Fontenay-Aux-Roses, France) (*14,16*), to create automatically a patient-specific voxel phantom. Tissue properties, such as the density and composition taken from International Commission on Radiological Protection (ICRP) 110 and 89 (*18,19*), were then attributed to each ROI of the voxel phantom using OEDIPE. Lungs density was set to 0.779 $g \cdot cm^{-3}$ and 0.752 $g \cdot cm^{-3}$ for men and women, respectively. NTL and TL densities were set to 1.05 $g \cdot cm^{-3}$ and RT density to 0.95 $g \cdot cm^{-3}$ for both men and women. For each patient, the lungs, NTL, and TL masses (m_{Lungs}, m_{NTL}, and m_{TL}, respectively) were estimated from the patient-specific voxel phantom and used to calculate the TB, defined as $\frac{m_{TL}}{m_{TL}+m_{NTL}}$.

Normalized Patient-Specific 3D Matrices of Cumulated Activity. The ^{99m}Tc SPECT/CT scan was first registered on the high-resolution CT scan using the Volumetrix software (GE Healthcare). Registered SPECT data were then used to generate a 3D matrix of disintegrations for the abdomen region. Because the 3D distribution of the ^{99m}Tc-MAA in the lungs is not known due to the lack of ^{99m}Tc SPECT/CT data for the whole thorax, the lung breakthrough (LB) was estimated from scintigraphy images using lungs and liver ROI. LB was defined as $LB = \frac{N_{Lungs}\, e^{\frac{dl}{2}(\mu_{Lungs}-\mu_{Liver})}}{N_{Liver}+N_{Lungs}\, e^{\frac{dl}{2}(\mu_{Lungs}-\mu_{Liver})}}$, where dl is the lung thickness, N_{ROI} is the number of counts in the ROI—calculated using the geometric mean of anterior and posterior counts—and μ_{Lungs} and μ_{Liver} are the linear attenuation coefficient for the lungs and the liver, respectively. For that study, standard ^{99m}Tc SPECT attenuation values were considered: dl = 20 cm, $\mu_{Lungs} = 0.04\ cm^{-1}$, and $\mu_{Liver} = 0.15\ cm^{-1}$ (*20*). Disintegrations, corresponding to this fixation to the lungs, were then homogeneously distributed in the lungs ROI. Finally, the 3D matrix was normalized to describe, in each voxel, the number of disintegrations, expressed in MBq·s, integrated over time for an injected activity of 1 GBq. The effective period of the radiopharmaceutical was considered equal to the physical half-life of ^{90}Y (64.1 h) because the microspheres are not biologically eliminated and remain implanted in the tissues.

Monte Carlo Simulations and Results Processing. MCNPX is a general-purpose transport code developed by Los Alamos National Laboratory (*17*). The MCNPX input file, in which the geometry is described using repeated structures, is provided automatically by OEDIPE. The ^{90}Y spectrum from ICRP 107 (*21*) was used for this study. Finally, the tally F6 was used in MCNPX to estimate the

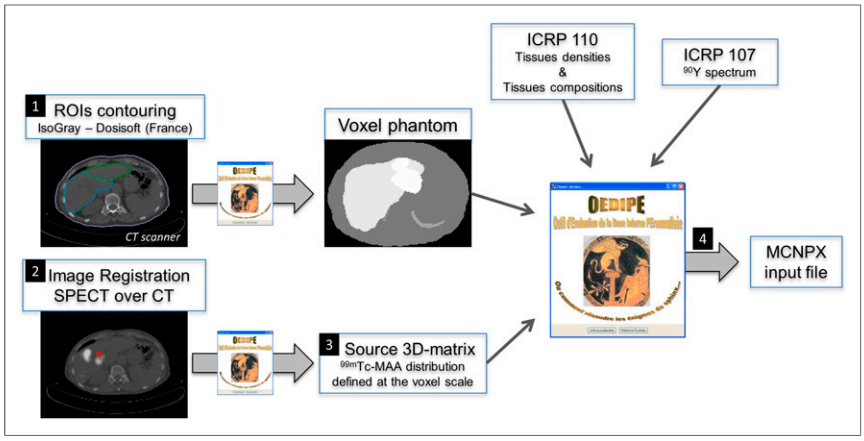

FIGURE 1. Methodology developed to generate MCNPX input file using OEDIPE software.

absorbed dose deposited in each voxel of the phantom. The complete methodology developed to generate the MCNPX input file from the patient initial data is illustrated in Figure 1. Monte Carlo calculations were performed using the 2.6c version of MCNPX on a Sun Fire X2200 node composed of 2 Opteron quad core processors with a 2.70 GHz CPU and 16 GB of RAM. At the end of Monte Carlo simulations, the MCNPX output file processing and analysis were performed using OEDIPE. Mean, minimum, and maximum absorbed doses in delineated ROI were calculated. Isodose curves superimposed on the voxel phantom were drawn, and DVHs were generated for each delineated ROI to provide valuable information for OAR radiation protection and tumor control.

MIA Calculations

OAR Tolerance Criteria. The MIA was defined as the maximum activity that could be injected to the patient that ensures OAR tolerance criteria are met. In practice, the activity actually injected to the patient will also depend on other clinical aspects, such as compromised liver status or the patient overall status. In general, tolerance criteria are based on D_{mean}. In clinical practice at HEGP, after considering toxicities reported in the literature for SIRT (*22,23*), mean absorbed dose limits for the lungs and NTL were set to 30 Gy ($D_{mean,NTL} \leq 30$ Gy and $D_{mean,Lungs} \leq 30$ Gy). Those values were thus considered for that retrospective study. However, because the lungs and the liver are parallel organs, a certain volume fraction can be highly irradiated without impairing the organ function, and tolerance criteria based on DVHs might be considered. Because no specific DVH tolerance criteria have been established for SIRT, theoretic tolerance criteria, inferred from external-beam radiotherapy follow-up, were considered in this study. For NTL, the DVH tolerance criterion states that the volume fraction of NTL receiving more than 30 Gy should be inferior to 50% ($V_{30\ Gy,NTL} \leq 50\%$) (*24*), whereas for the lungs, it relies on 2 simultaneous conditions (*24*): the volume fractions of lungs receiving more than 20 and 30 Gy, respectively, should be inferior to 35% ($V_{20\ Gy,Lungs} \leq 35\%$) and 20% ($V_{30\ Gy,Lungs} \leq 20\%$). Because tolerance criteria are defined from absorbed doses, the MIA was calculated in 3 different ways depending on the dosimetric method and the type of tolerance criteria: PM and D_{mean}, PMCD and D_{mean}, and PMCD and DVHs.

PM. The PM is based on the MIRD schema for radiopharmaceutical dosimetry (*8*). For ^{90}Y, the absorbed dose to an ROI (NTL, TL, or lungs), in Grays, is given as $D_{MIRD,ROI} = \frac{49,670}{m_{ROI}} A_{ROI}$, where m_{ROI} is the ROI mass in grams, and A_{ROI} is the activity in the ROI in gigabecquerels. For each evaluation, ROI masses and activities were thus determined using OEDIPE from the patient-specific phantoms and 3D matrices of activity. The MIA (PM and D_{mean}) was then deduced using D_{mean} tolerance criteria for the lungs and NTL. Finally, the tumor–to–normal-tissue ratio (T/N), defined as $\frac{T}{N} = \frac{A_{TL}}{A_{NTL}} \times \frac{m_{NTL}}{m_{TL}}$, was calculated to characterize the differential of fixation between TL and NTL.

PMCD. DVHs of the lungs and NTL, along with the associated D_{mean}, were obtained for an injected activity of 1 GBq from the processing of the MCNPX output file. Additional tools were developed in OEDIPE to calculate, from these results, the MIAs associated to tolerance criteria based on either D_{mean} or DVHs.

The results presented in this article were obtained from MCNPX simulations with 100 million histories. MIAs calculated using these simulations were set as the reference. To study the impact of the number of simulated histories on the MIA calculation, additional simulations were run for 1, 10, 25, and 50 million histories. The relative error on MIA determination for a n-million-histories simulation (MIA_{nM}), compared with the reference (MIA_{100M}), was defined as $RE = \frac{|MIA_{100M} - MIA_{nM}|}{MIA_{100M}}$.

Absorbed Dose Calculations

Because the PMCD provides a more accurate dosimetry than the PM, the OEDIPE software was finally used to calculate absorbed doses at the voxel scale, which could be delivered if the different values of MIA were injected to the patient. These calculations do not require additional Monte Carlo calculations because MCNPX output files can be processed by the OEDIPE software for any value of injected activity. Finally, mean, minimum, and maximum absorbed doses were calculated with the OEDIPE software from all these absorbed dose distributions.

To characterize the cross-fire between the abdomen and the lungs, MCNPX simulations without lungs fixation were run. D_{mean} to the lungs, NTL, and TL were calculated from the simulations with lung counts ($D_{ref,ROI}$) and from the simulations without lungs counts ($D_{woLungs,ROI}$). The cross-fire from the abdomen (NTL, TL, and RT, i.e., the remaining tissues) to the lungs was defined as $\%D_{Lungs \leftarrow TL+NTL+RT} = D_{woLungs,Lungs}/D_{ref,Lungs}$, and the cross-fire from the lungs to another ROI, either NTL or TL, was defined as $\%D_{ROI \leftarrow Lungs} = (D_{ref,ROI} - D_{woLungs,ROI})/D_{ref,ROI}$.

RESULTS

Patients and Evaluations Characteristics

Whole-liver and TL masses, TB, T/N ratio, and LB values are reported in Table 1. Whole-liver and TL masses ranged, respectively, from 1,287 to 5,823 g and from 46 to 2,887 g. The variability in TB, T/N ratio, and LB was broad. TB values ranged from 3% to 54%. T/N ratios ranged from 0.65 to 3.91, with a mean value of 1.89 ± 0.94, and LB ranged from 0% to 7.22%, with a mean value of 2.47% ± 2.07%.

MIA

The results obtained for MIA calculations, depending on the dosimetric method and the tolerance criteria, are presented in Table 2. For all evaluations, the MIA increases with the method accuracy or with the tolerance criteria sophistication. For D_{mean} tolerance criteria, the ratio between the MIA recommended by the PMCD and the one recommended by the PM was, in average, of 1.27 ± 0.14 over all evaluations, with values ranging from 1.11 to 1.65. When only the PMCD method was considered, the

TABLE 1
Patients and Evaluations Characteristics

Treatment type	Patient	Evaluation	WL mass (g)	TL mass (g)	TB (%)	T/N ratio	LB (%)
WLI	P1	E1	2,701	631	23	0.65	2.16
	P1	E2	2,701	631	23	0.88	2.23
	P2	E3	2,145	229	11	1.89	2.36
	P3	E4	2,751	1,432	52	2.90	7.22
	P4	E5	1,287	66	5	2.23	0
	P5	E6	2,165	458	21	1.61	0
RLI	P6	E7	1,777	726	41	1.01	0
	P7	E8	5,367	2,887	54	1.73	3.56
	P8	E9	1,544	46	3	1.06	1.20
	P9	E10	1,444	102	7	2.66	3.16
LLI	P2	E11	2,145	229	11	3.91	3.53
	P3	E12	2,751	1,432	52	2.84	4.99
	P10	E13	5,823	2,662	46	1.10	3.50
	P8	E14	1,544	46	3	1.95	0.73
Mean ± SD			2,700 ± 1,606 (n = 10)	924 ± 1,061 (n = 10)	26 ± 20 (n = 10)	1.89 ± 0.94 (n = 14)	2.47 ± 2.07 (n = 14)

ratio between the MIA based on DVHs and the one based on D_{mean} ranged from 1.12 to 1.94, with a mean of 1.32 ± 0.24 over whole-liver irradiation (WLI) and right lobe irradiation (RLI) evaluations. For left lobe irradiation (LLI) evaluations, that ratio can reach 7.79, with a mean of 5.33 ± 2.26. Finally, the variability of the ratio between the MIA based on the PMCD with DVHs and the one based on the PM with D_{mean} was broad. That ratio ranged from 1.40 to 12.88, with a mean of 1.64 ± 0.21 over WLI and RLI evaluations and of 7.40 ± 4.22 over LLI evaluations.

3D PMCD

Isodose curves superimposed on the voxel phantom were obtained for each evaluation. Figure 2 displays examples of isodose curves obtained for evaluation E3 with an injected activity of 1 GBq. Isodose curves of highest values (45, 50, and 55 Gy) are located in the TL.

Moreover, DVHs were calculated for each evaluation for TL and the 3 OAR (NTL, right lung, and left lung). Characteristic examples of DVHs obtained for an injected activity of 1 GBq are shown in Figure 3. First, TL DVHs are clearly shifted toward

TABLE 2
Comparison of MIA Values Depending on Chosen Approach

Treatment type	Evaluation	MIA (GBq)			$\frac{MIA_{PMCD,D_{mean}}}{MIA_{PM,D_{mean}}}$	$\frac{MIA_{PMCD,DVHs}}{MIA_{PMCD,D_{mean}}}$	$\frac{MIA_{PMCD,DVHs}}{MIA_{PM,D_{mean}}}$
		PM,D_{mean}*	PMCD,D_{mean}†	PMCD,DVHs‡			
WLI	E1	1.53	1.88	2.57	1.23	1.37	1.68
	E2	1.62	2.13	2.75	1.31	1.29	1.70
	E3	1.45	1.93	2.16	1.33	1.12	1.49
	E4	3.56	3.95	7.65	1.11	1.94	2.15
	E5	0.83	1.12	1.41	1.35	1.26	1.70
	E6	1.48	1.74	2.26	1.18	1.30	1.53
RLI	E7	1.08	1.33	1.51	1.23	1.14	1.40
	E8	4.68	5.39	7.83	1.15	1.45	1.67
	E9	0.95	1.27	1.42	1.34	1.12	1.49
	E10	1.01	1.30	1.63	1.29	1.25	1.61
LLI	E11	1.76	2.91	22.7	1.65	7.79	12.9
	E12	3.42	3.81	11.1	1.11	2.91	3.25
	E13	3.81	4.88	19.5	1.28	3.99	5.12
	E14	0.97	1.23	8.13	1.27	6.61	8.38
All types (n = 14)	Mean ± SD	2.01 ± 1.28	2.49 ± 1.45	6.62 ± 6.93	1.27 ± 0.14	2.47 ± 2.18	3.29 ± 3.39
WLI and RLI (n = 10)	Mean ± SD	1.82 ± 1.27	2.20 ± 1.38	3.12 ± 2.48	1.25 ± 0.08	1.32 ± 0.24	1.64 ± 0.21
LLI (n = 4)	Mean ± SD	2.49 ± 1.35	3.21 ± 1.54	15.36 ± 6.87	1.33 ± 0.23	5.33 ± 2.26	7.41 ± 4.23

MIAs obtained with:
*PM and D_{mean} tolerance criteria.
†PMCD and D_{mean} tolerance criteria.
‡PMCD and DVH tolerance criteria.

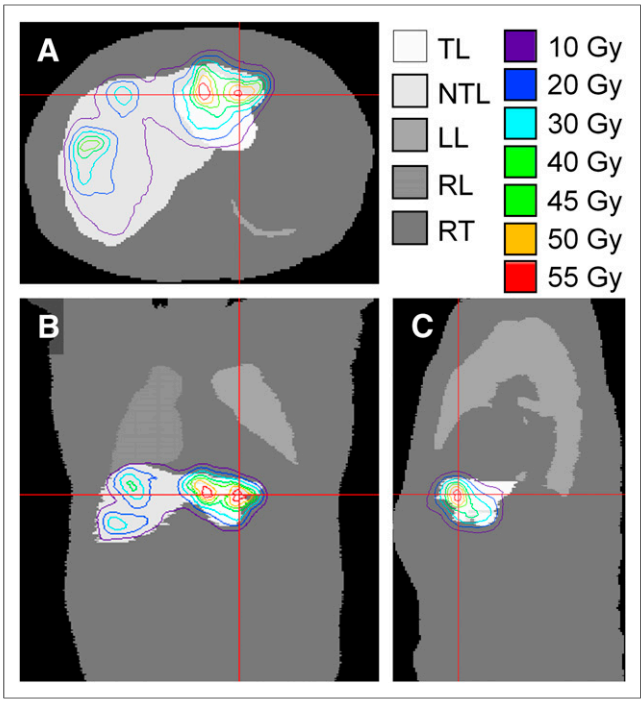

FIGURE 2. Axial (A), coronal (B), and sagittal (C) views of isodose curves superimposed on patient-specific voxel phantom obtained for evaluation E3 with an injected activity of 1 GBq. LL = left lung; RL = right lung.

higher doses, compared with NTL DVHs, confirming the treatment selectivity. Second, as expected, the shapes of NTL DVHs are different depending on the treatment type (Fig. 3). In fact, the drop along the *y*-axis of the NTL DVH is much steeper for RLI and LLI than for WLI. This difference is related to the nontreated NTL volume in lobar treatments. Finally, on Figure 3, the shapes of the lungs DVHs show that a large proportion of lungs voxels receive negligible absorbed doses. Figure 4 shows the lungs DVHs obtained for an injected activity of 3.95 GBq—the MIA recommended by the PMCD with D_{mean} tolerance criteria—for evaluation E4 for which the LB was substantial (7.22%). For that evaluation, 95% and 5% of the lungs volume received more than 2.4 and 5.0 Gy, respectively.

Finally, absorbed doses at the voxel scale were calculated with the PMCD method for the 3 values of MIA reported in Table 2. The mean and range of these absorbed doses are reported in Tables 3–5 for the NTL, lungs, and TL, respectively. The mean and SD over all evaluations, over WLI and RLI, and over LLI are reported in the same tables. The fractions of NTL and TL absorbed dose due to cross-fire from the lungs are reported in Tables 3 and 5, respectively. The fraction of the lung absorbed dose due to cross-fire from NTL, TL, and RT is reported in Table 4.

Finally, relative errors on MIA determination with regard to the number of simulated histories, compared with the 100-million-histories simulations, are reported in Figure 5. For the MIA recommended by the PMCD with D_{mean} tolerance criteria (Fig. 5A), relative errors were inferior to 0.6% for the 10-million-histories simulations. For the MIA recommended by the PMCD with DVH tolerance criteria (Fig. 5B), relative errors were inferior to 4.6% and 1.5% for the 10-million- and 25-million-histories simulations, respectively. Relative errors reach a stable value for simulations from 25 million of histories.

DISCUSSION

The interest of patient-specific voxel phantoms was confirmed by the fact that whole liver masses are predominantly higher than the reference masses for men and women (*18*), and their variability

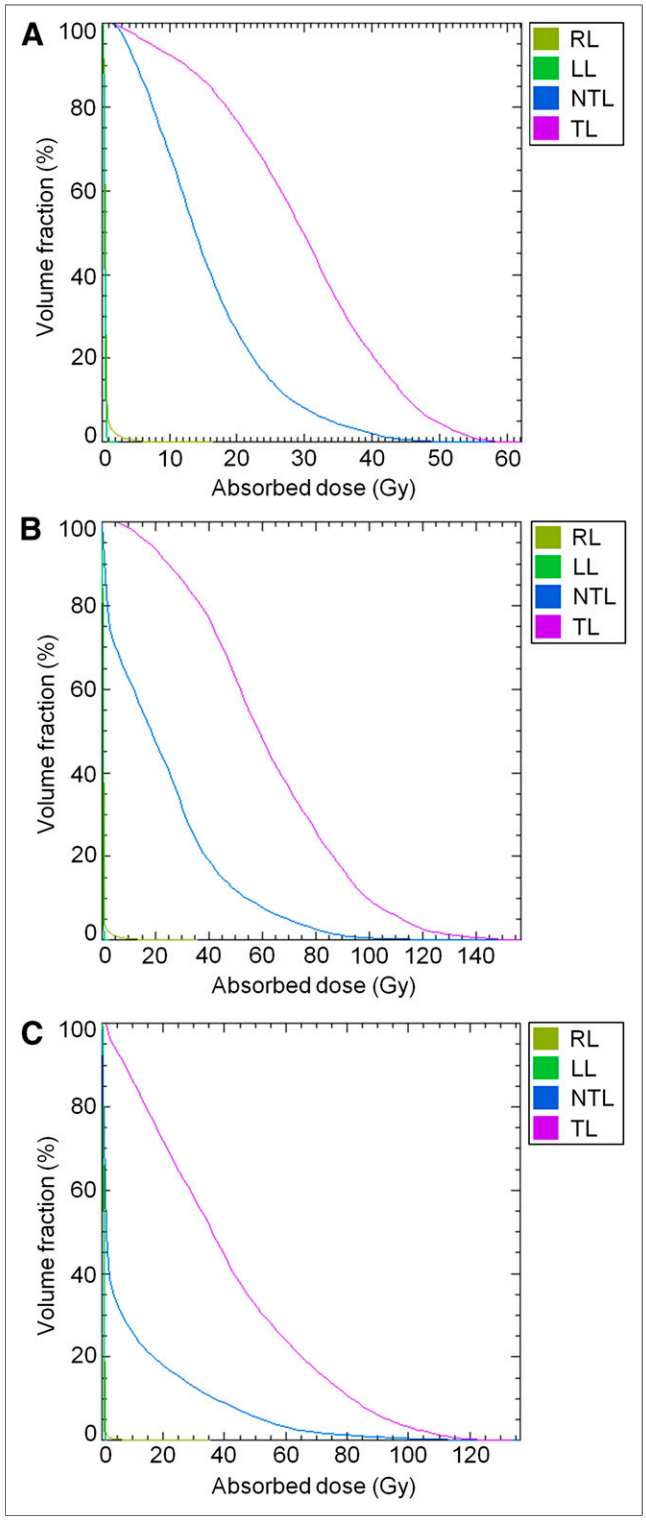

FIGURE 3. DVHs for RL, LL, NTL, and TL obtained for evaluation E3 (A), E10 (B), and E11 (C) with an injected activity of 1 GBq. LL = left lung; RL = right lung.

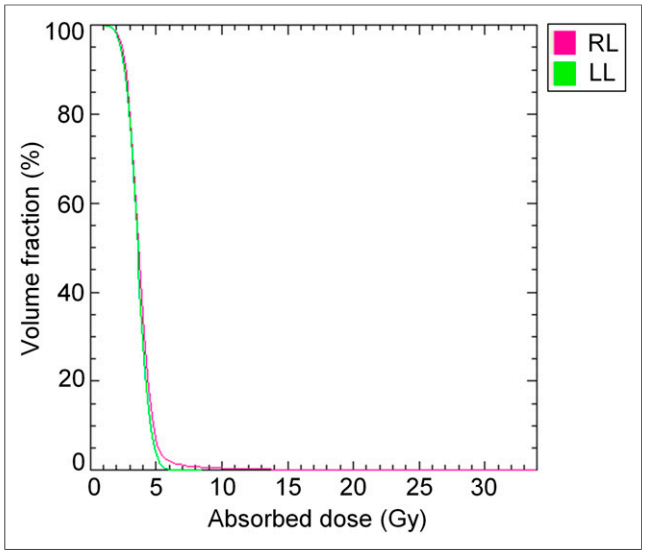

FIGURE 4. DVHs for RL and LL obtained for evaluation E4 with an injected activity of 3.95 GBq. LL = left lung; RL = right lung.

over patients is broad. This study also stresses the strong disparity in the values of T/N ratio. No correlation was found between the T/N ratio and the TB or the treatment type (WLI, LLI, RLI). This point correlates with previous publications highlighting the influence of hepatic vascularization on the fixation differential (*23*). From an optimization point of view, this result also emphasizes the interest of methods, such as the PM and 3D personalized methods, which integrate the fixation differential into the determination of the activity to be injected. Finally, for patients who underwent two ^{99m}Tc-MAA evaluations successively, the LB varied from one evaluation to the next, implying that the LB has to be reevaluated each time the injecting conditions are changed.

Regarding calculation time, after, respectively, 7 and 17 h on 1 node, 10-million- and 25-million-histories simulations achieved errors of less than 5% and 1.5%, respectively (Fig. 5), compared with the 100-million-histories simulations. Because the time period between the last ^{99m}Tc evaluation and the ^{90}Y treatment was around 15 d, those calculation times are thus perfectly acceptable for clinical routine.

The influence of the dosimetric method on activity prescription is highlighted by the comparison between MIAs obtained with the PM and the PMCD using D_{mean} tolerance criteria. For all evaluations, the MIA estimated with the PMCD was superior to the one estimated with the PM, confirming that tolerance criteria are met for PM recommendations which are thus conservative. Moreover, the PMCD, which accounts for both fixation heterogeneities and cross-fire, contributes toward treatment optimization.

The advantages of DVHs for treatment optimization and personalization are highlighted by the comparison between MIAs obtained with the PMCD for tolerance criteria on either D_{mean} or DVHs. In fact, for all evaluations, the MIAs estimated with DVH tolerance criteria were higher and more spread out than the ones with D_{mean} tolerance criteria. Their ratio was equal to 1.32 ± 0.24 for WLI and RLI evaluations and 5.33 ± 2.26 for LLI evaluations. For WLI and RLI evaluations—excluding E4 and E8, which are particular cases—MIAs obtained using the PMCD with DVH tolerance criteria ranged from 1.41 to 2.75 GBq, a standard range in clinical practice. For evaluations E4 and E8, all 3 methods recommend much higher activities than for other WLI and RLI evaluations, a difference that can be explained by large liver volumes combined with important TB for these patients. For LLI evaluations, MIAs obtained using the PMCD with DVH tolerance criteria ranged from 8.13 to 22.7 GBq; these high values are explained by the fact that, because the left lobe represents around one third of the whole liver volume, the injected activity could be increased significantly while still ensuring a $V_{30\ Gy}$ less than 50%. Moreover, the 2 highest values were obtained for patients with a low TB and lesions mainly located in the left lobe. If injected, these activities would certainly lead to left lobectomy (*25*). Thus, depending on the therapy intent, a tolerance criterion on left lobe instead of whole liver could be considered to avoid left lobectomy. Furthermore, MIA determination only relied on OAR dosimetry considerations. In clinical practice, other considerations, such as a cirrhotic liver, could be more restrictive than OAR dosimetry. Therefore, by taking advantage of the parallel characteristic of the liver, DVH tolerance criteria can lead to an increase of the injected activity, which is more or less important depending on the patient.

Finally, the complete benefit brought by the PMCD, compared with the PM, is illustrated by the comparison of the MIAs obtained with the PMCD and DVH tolerance criteria and the ones obtained with the PM. Thanks to the combination of accurate absorbed dose calculations with elaborate tolerance criteria, the PMCD allows an increase of at least 40% of the injected activity and is thus of high interest for strongly personalized treatment optimization.

Regarding NTL absorbed doses, the cross-fire contribution from the lungs to D_{mean} ($D_{mean,NTL}$) was negligible, ranging from 0% to 0.13%. However, the reliability of these results is conditioned to the assumption of homogeneity for the lungs' activity distribution. For the MIA based on PM, $D_{mean,NTL}$ values were significantly

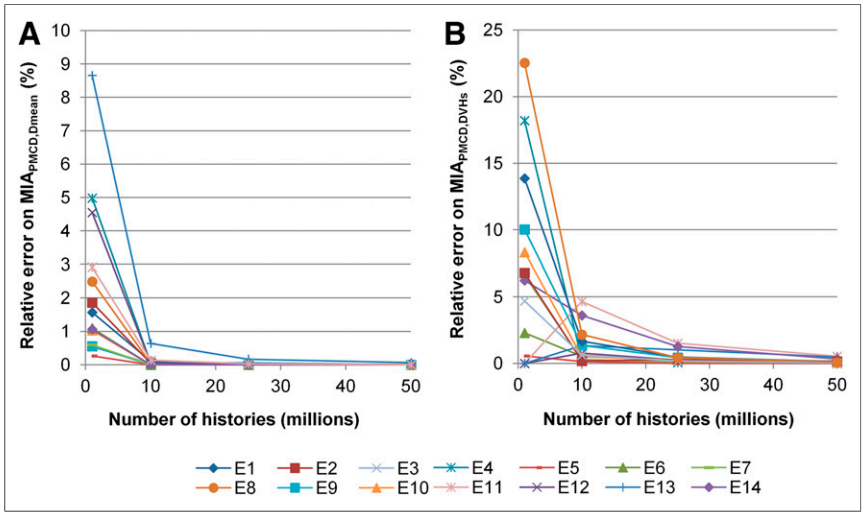

FIGURE 5. Relative errors on MIA determination for D_{mean} tolerance criteria (A) and DVH tolerance criteria (B) for all 14 evaluations with regard to number of histories simulated in MCNPX calculations.

TABLE 3
Absorbed Doses to NTL and Cross-Fire Fraction

Treatment type	Evaluation	%$D_{NTL \leftarrow Lungs}$* (%)	Absorbed doses to NTL (Gy)		
			MIA (PM,D_{mean})	MIA (PMCD,D_{mean})	MIA (PMCD,DVHs)
WLI	E1	0.00	24.4 (0–2.5 × 10^2)	30.0 (0–3.1 × 10^2)	41.0 (0–4.3 × 10^2)
	E2	0.00	22.8 (0–1.0 × 10^2)	30.0 (0–1.3 × 10^2)	38.6 (0–1.7 × 10^2)
	E3	0.02	22.6 (0.8–8.4 × 10^1)	30.0 (1.0–1.1 × 10^2)	33.5 (1.1–1.2 × 10^2)
	E4	0.13	27.1 (0–4.9 × 10^2)	30.0 (0–5.4 × 10^2)	58.1 (0–1.0 × 10^3)
	E5	0.00	22.1 (0–1.2 × 10^2)	30.0 (0–1.7 × 10^2)	37.7 (0–2.1 × 10^2)
	E6	0.00	25.5 (0–1.9 × 10^2)	30.0 (0–2.3 × 10^2)	39.1 (0–2.9 × 10^2)
RLI	E7	0.00	24.2 (0–8.8 × 10^2)	30.0 (0–1.1 × 10^2)	34.1 (0–1.2 × 10^2)
	E8	0.11	26.0 (0–1.3 × 10^2)	30.0 (0–1.5 × 10^2)	43.5 (0–2.1 × 10^2)
	E9	0.00	22.4 (0–1.3 × 10^2)	30.0 (0–1.7 × 10^2)	33.6 (0–1.9 × 10^2)
	E10	0.01	23.3 (0–1.5 × 10^2)	30.0 (0–2.0 × 10^2)	37.8 (0–2.5 × 10^2)
LLI	E11	0.01	18.2 (0–2.4 × 10^2)	30.0 (0–4.0 × 10^2)	234 (0–3.1 × 10^3)
	E12	0.07	27.0 (0–1.0 × 10^3)	30.0 (0–1.1 × 10^3)	87.4 (0–3.2 × 10^3)
	E13	0.07	23.4 (0–2.3 × 10^2)	30.0 (0–3.0 × 10^2)	120 (0–1.2 × 10^3)
	E14	0.01	23.6 (0–1.6 × 10^2)	30.0 (0–2.1 × 10^2)	199 (0–1.4 × 10^3)
All types (n = 14)	Mean ± SD	0.03 ± 0.04	23.8 ± 2.29	30.0 ± 0.0	74.1 ± 65.5
WLI and RLI (n = 10)	Mean ± SD	0.03 ± 0.05	24.0 ± 1.70	30.0 ± 0.0	39.7 ± 7.23
LLI (n = 4)	Mean ± SD	0.04 ± 0.03	23.1 ± 3.63	30.0 ± 0.0	160 ± 68.0

*Cross-fire contribution from the lungs fixation to NTL.

lower than the tolerance dose of 30 Gy and quite variable irrespective of treatment type. For the MIA based on the PMCD with D_{mean} tolerance criteria, $D_{mean,NTL}$ values were equal to 30.0 Gy for all evaluations, reflecting the fact that the lungs tolerance criterion was less restrictive than that of NTL. For the MIA based on the PMCD with DVH tolerance criteria, $D_{mean,NTL}$ values ranged from 33.5 to 234 Gy. Those values, which are superior to the NTL tolerance criterion based on D_{mean}, illustrate the limitation of D_{mean} tolerance criteria that do not take advantage of the parallel characteristics of the liver and the lungs. $D_{mean,NTL}$ values obtained for LLI evaluations (87.4–234 Gy) may seem important, compared with the ones obtained for WLI and RLI evaluations (33.5–58.1 Gy). However, because a significant NTL fraction is spared in lobar treatments, $D_{mean,NTL}$ is not representative of NTL irradiation. In fact, in left lobe treatments, the DVH tolerance criterion for NTL ($V_{30\ Gy} < 50\%$) is met, even with a high D_{mean}.

Regarding lungs absorbed doses, D_{mean} ($D_{mean,Lungs}$) does not exceed 4.04 Gy for the MIAs calculated using D_{mean} tolerance

TABLE 4
Absorbed Doses to Lungs and Cross-Fire Fraction

Treatment type	Evaluation	%$D_{Lungs \leftarrow TL + NTL + RT}$* (%)	Absorbed doses to the lungs (Gy)		
			MIA (PM,D_{mean})	MIA (PMCD,D_{mean})	MIA (PMCD,DVHs)
WLI	E1	20	0.48 (0–3.5 × 10^1)	0.58 (0–4.3 × 10^1)	0.80 (0–5.9 × 10^1)
	E2	22	0.54 (0–4.1 × 10^1)	0.71 (0–5.4 × 10^1)	0.91 (0–7.0 × 10^1)
	E3	14	0.71 (0–2.4 × 10^1)	0.94 (0–3.1 × 10^1)	1.05 (0–3.5 × 10^1)
	E4	4	3.32 (0–3.1 × 10^1)	3.68 (0–3.4 × 10^1)	7.14 (0–6.6 × 10^1)
	E5	100	0.14 (0–4.5 × 10^1)	0.19 (0–6.1 × 10^1)	0.24 (0–7.6 × 10^1)
	E6	100	0.08 (0–4.4 × 10^1)	0.10 (0–5.2 × 10^1)	0.13 (0–6.8 × 10^1)
RLI	E7	100	0.31 (0–4.4 × 10^1)	0.38 (0–5.4 × 10^1)	0.43 (0–6.1 × 10^1)
	E8	11	3.51 (0.6–5.3 × 10^1)	4.04 (0.7–6.1 × 10^1)	5.87 (1.0–8.9 × 10^1)
	E9	27	0.22 (0–1.9 × 10^1)	0.29 (0–2.5 × 10^1)	0.33 (0–2.8 × 10^1)
	E10	19	0.50 (0–3.6 × 10^1)	0.64 (0–4.6 × 10^1)	0.81 (0–5.8 × 10^1)
LLI	E11	6	1.16 (0–6.2 × 10^1)	1.92 (0–1.0 × 10^2)	15.0 (0–8.0 × 10^2)
	E12	4	2.20 (0–2.5 × 10^1)	2.45 (0–2.8 × 10^1)	7.14 (0–8.2 × 10^1)
	E13	3	1.57 (0–2.9 × 10^1)	2.01 (0–3.8 × 10^1)	8.03 (0–1.5 × 10^2)
	E14	48	0.19 (0–4.0 × 10^1)	0.24 (0–5.1 × 10^1)	1.60 (0–3.4 × 10^2)
All types (n = 14)	Mean ± SD	34 ± 38	1.07 ± 1.16	1.30 ± 1.31	3.53 ± 4.45
WLI and RLI (n = 10)	Mean ± SD	42 ± 41	0.98 ± 1.30	1.16 ± 1.45	1.77 ± 2.53
LLI (n = 4)	Mean ± SD	15 ± 22	1.28 ± 0.84	1.66 ± 0.97	7.94 ± 5.50

*Cross-fire contribution from NTL, TL, and RT fixations to the lungs.

TABLE 5
Absorbed Doses to TL and Cross-Fire Fraction

Treatment type	Evaluation	$\%D_{TL\leftarrow Lungs}$* (%)	Absorbed doses to TL (Gy)		
			MIA (PM,D_{mean})	MIA (PMCD,D_{mean})	MIA (PMCD,DVHs)
WLI	E1	0.08	15.9 (0–9.7 × 10^1)	19.5 (0–1.2 × 10^2)	26.6 (0–1.6 × 10^2)
	E2	0.00	20.4 (0–9.2 × 10^1)	26.8 (0–1.2 × 10^2)	34.5 (0–1.6 × 10^2)
	E3	0.01	42.6 (1.4–9.0 × 10^1)	56.6 (1.8–1.2 × 10^2)	63.3 (2.0–1.3 × 10^2)
	E4	0.01	77.7 (0–5.2 × 10^2)	86.2 (0–5.8 × 10^2)	167 (0–1.1 × 10^3)
	E5	0.00	49.2 (2.9–1.4 × 10^2)	66.9 (3.9–1.9 × 10^2)	83.9 (4.9–2.4 × 10^2)
	E6	0.00	40.9 (0.2–1.9 × 10^2)	48.1 (0.2–2.2 × 10^2)	62.6 (0.2–2.9 × 10^2)
RLI	E7	0.00	24.6 (0–8.9 × 10^1)	30.5 (0.1–1.1 × 10^2)	34.6 (0.1–1.2 × 10^2)
	E8	0.00	45.1 (0–1.6 × 10^2)	52.0 (0–1.9 × 10^2)	75.5 (0–2.7 × 10^2)
	E9	0.04	23.5 (2.5–1.2 × 10^2)	31.5 (3.4–1.6 × 10^2)	35.3 (3.8–1.8 × 10^2)
	E10	0.05	62.0 (2.9–1.6 × 10^2)	79.9 (3.8–2.0 × 10^2)	101 (4.8–2.6 × 10^2)
LLI	E11	0.02	71.3 (1.3–2.4 × 10^2)	118 (2.1–3.9 × 10^2)	918 (16–3.0 × 10^3)
	E12	0.02	76.0 (0–1.2 × 10^3)	84.6 (0–1.3 × 10^3)	246 (0–3.9 × 10^3)
	E13	0.01	25.6 (0–2.3 × 10^2)	32.8 (0–3.0 × 10^2)	131 (0–1.2 × 10^3)
	E14	0.08	46.2 (0.01–1.1 × 10^2)	58.8 (0.01–1.5 × 10^2)	389 (0.1–9.7 × 10^2)
All types (n = 14)	Mean ± SD	0.02 ± 0.03	44.4 ± 21.0	56.6 ± 28.2	169 ± 238
WLI and RLI (n = 10)	Mean ± SD	0.02 ± 0.03	40.2 ± 19.7	49.8 ± 22.9	68.4 ± 42.5
LLI (n = 4)	Mean ± SD	0.03 ± 0.03	54.8 ± 23.4	73.6 ± 36.4	421 ± 348

*Cross-fire contribution from the lungs to TL.

criteria. For MIAs calculated with DVH tolerance criteria, $D_{mean,Lungs}$ values ranged from 0.13 to 15.0 Gy. Therefore, even if our experience shows that the lungs irradiation is not the restricting criterion, $D_{mean,Lungs}$ can be significant for some evaluations. Finally, D_{mean} to the lungs due to cross-fire from NTL, TL, and RT ranged from 0.09 to 0.88 Gy. However, even if these values are low, it is important to remember that, because the lungs fixation is unknown, we assumed a homogeneous distribution for lungs self-absorption calculations. In fact, Figure 4 shows that, because of cross-fire, the maximal dose to the lungs reached 34 Gy and that 5% of the lungs receive a dose higher than 5.0 Gy. Thus, if, in reality, the lungs activity is concentrated in their lower parts, even higher doses might be reached in these locations.

Regarding TL absorbed doses, the cross-fire contribution from the lungs to D_{mean} ($D_{mean,TL}$) was negligible, ranging from 0% to 0.08%. For the MIA based on PM, $D_{mean,TL}$ values ranged from 15.9 to 77.7 Gy, and a high variability was observed irrespective of treatment type. For the MIA based on the PMCD with D_{mean} tolerance criteria, $D_{mean,TL}$ values ranged from 19.5 to 118 Gy. Those values are of the same order of magnitude than values reported by Flamen et al. (*26*) for liver metastases treated using SIR-Spheres but are much lower than the ones published by Dieudonné et al. (*11*) for HCC dosimetry based on dose kernels, which ranged from 244 to 1,190 Gy. That difference could be first explained by the easiest targeting of HCC, compared with hepatic metastases, which are much more diffuse lesions. That difference could also be related to the segmentation technique used to define the TL volume, which is based on thresholding of SPECT data in the Dieudonné et al. (*11*) study. On the contrary, in that study, TL volume was segmented on CT images without a priori on the activity distribution. For the MIA calculated using DVH tolerance criteria, $D_{mean,TL}$ values ranged from 26.6 to 918 Gy. Therefore, using tolerance criteria on DVHs allow the delivery of higher doses to TL while preserving OAR functions. Finally, as representations of the absorbed dose distribution, isodose curves and DVHs could also be used to foresee the response to treatment. In fact, isodose curves can be used to identify lesions with high or low irradiation, whereas DVHs, along with minimum and maximum absorbed doses, can be calculated for each lesion independently.

Finally, it would be of interest to perform, for the same pool of patients, a dosimetry using dose kernel techniques, because these can provide good estimates of absorbed doses to the liver with shorter calculation times once the technique is implemented with kernels calculated for the right pixel size. Moreover, SPECT reconstruction was performed with the clinical protocol established for ^{99m}Tc at HEGP because it was used for partition model calculations in clinical routine. Because the Hann postfiltering might introduce a bias due to the loss in spatial resolution, it could be interesting to look at the impact on dosimetry of this filter, compared with more quantitative filters. Furthermore, future developments of the methodology could include estimations of absorbed doses to other OAR such as the stomach or gallbladder. Moreover, to verify the assumption of similarity between MAA and microsphere distributions, the application of the PMCD method to perform postdosimetry using ^{90}Y SPECT or ^{90}Y PET data would be valuable. MIA determination would also benefit from more knowledge on the activity distribution in the lungs and on the hepatic and pulmonary tolerances to internal irradiation to better define OAR tolerance criteria for SIRT. In fact, at the moment, the only DVH tolerance criteria available are the ones deducted from external-beam radiotherapy follow-up, which may not reflect the irradiation delivered by SIRT. A dose–effect relationship, characteristic of SIRT, would thus be of great interest for both OAR radiation protection and tumoral response.

CONCLUSION

A 3D treatment plan, based on Monte Carlo calculations and patient-specific data on anatomy and activity distribution, was developed using the OEDIPE software. With a treatment optimization

purpose, this personalized dosimetry was performed for fourteen ^{99m}Tc-MAA evaluations in the context of SIRT. The PMCD dosimetry combined with DVH tolerance criteria makes treatment optimization possible. Absorbed doses to TL were maximized for each patient depending on its evaluation, thus leading to potentially better treatment efficiency.

DISCLOSURE

The costs of publication of this article were defrayed in part by the payment of page charges. Therefore, and solely to indicate fact, this article is hereby marked "advertisement" in accordance with 18 USC section 1734. No potential conflict of interest relevant to this article was reported.

REFERENCES

1. Ferlay J, Shin HR, Bray F, Forman D, Mathers C, Parkin DM. Estimates of worldwide burden of cancer in 2008: GLOBOCAN 2008. *Int J Cancer.* 2010; 127:2893–2917.
2. Young A, Rea D. ABC of colorectal cancer: treatment of advanced disease. *BMJ.* 2000;321:1278–1281.
3. Vibert E, Canedo L, Adam R. Strategies to treat primary unresectable colorectal liver metastases. *Semin Oncol.* 2005;32:33–39.
4. Llovet JM, Burroughs A, Bruix J. Hepatocellular carcinoma. *Lancet.* 2003;362: 1907–1917.
5. Khodjibekova M, Szyszko T, Khan S, Nijran K, Tait P, Al-Nahhas A. Selective internal radiation therapy with yttrium-90 for unresectable liver tumours. *Rev Recent Clin Trials.* 2007;2:212–216.
6. Sirtex Medical. *Sirtex Medical Training Manual: Training Program Physicians and Institutions*. Lane Cove, New South Wales, Australia: Sirtex Medical.
7. Ho S, Lau WY, Leung TW, et al. Partition model for estimating radiation doses from yttrium-90 microspheres in treating hepactic tumours. *Eur J Nucl Med.* 1996;23:947–952.
8. Gulec SA, Mesoloras G, Stabin M. Dosimetric techniques in ^{90}Y-microsphere therapy of liver cancer: the MIRD equations for dose calculations. *J Nucl Med.* 2006;47:1209–1211.
9. Kolbert KS, Sgouros G, Scott AM, et al. Implementation and evaluation of patient-specific three-dimensional internal dosimetry. *J Nucl Med.* 1997;38:301–308.
10. Sarfaraz M, Kennedy AS, Lodge MA, Li XA, Wu X, Yu CX. Radiation absorbed dose distribution in a patient treated with yttrium-90 microspheres for hepatocellular carcinoma. *Med Phys.* 2004;31:2449–2453.
11. Dieudonné A, Garin E, Laffont S, et al. Clinical feasibility of fast 3-dimentional dosimetry of the liver for treatment planning of hepatocellular carcinoma. *J Nucl Med.* 2011;52:1930–1937.
12. Zaidi H, Andreo P. Monte Carlo techniques in nuclear medicine dosimetry. In: Zaidi H, Sgouros G, eds. *Therapeutic Applications of Monte Carlo Calculations in Nuclear Medicine*. Philadelphia, PA: Institute of Physics Publishing; 2002:28–54.
13. Stabin MG, Bardiès M. Applications to Nuclear Medicine. In: Xu XG, Eckerman, eds. *Handbook of Anatomical Models for Radiation Dosimetry.* Boca Raton, FL: CRC Press; 2009:471-486.
14. Chiavassa S, Aubineau-Lanièce I, Bitar A, et al. Validation of a personalized dosimetric evaluation tool (Oedipe) for targeted radiotherapy based on the Monte Carlo MCNPX code. *Phys Med Biol.* 2006;51:601–616.
15. Hobbs RF, Wahl RL, Lodge MA, et al. ^{124}I PET-based 3D-RD dosimetry for a pediatric thyroid cancer patient: real-time treatment planning and methodologic comparison. *J Nucl Med.* 2009;50:1844–1847.
16. Chiavassa S, Bardies M, Guiraud-Vitaux F, et al. OEDIPE: a personalized dosimetric tool associating voxel-based models with MCNPX. *Cancer Biother Radiopharm.* 2005;20:325–332.
17. Pelowitz DB. *MCNPX User's Manual Version 2.6.0.* Technical report LA-CP-05-0369. Los Alamos, NM: Los Alamos National Laboratory; 2008.
18. International Commission on Radiological Protection (ICRP). *Adult Reference Computational Phantoms*. ICRP publication 110. Oxford, U.K.: Elsevier; 2009.
19. International Commission on Radiological Protection (ICRP). *Basic Anatomical and Physiological Data for Use in Radiological Protection: Reference Values*. ICRP publication 89. Stockholm, Sweden: Pergamon; 2002.
20. Buvat I. MSc in biological and medical engineering: quantification in emission tomography. U494 INSERM. http://www.guillemet.org/irene/coursem/creteil.pdf. Accessed December 28, 2013.
21. International Commission on Radiological Protection (ICRP). *Nuclear Decay Data for Dosimetric Calculations*. ICRP publication 107. Oxford, U.K.: Elsevier; 2008.
22. Inarrairaegui M, Sangro B. Results in hepatocellular carcinoma. In: Bilbao JI, Reiser MF, eds. *Liver Radioembolisation with ^{90}Y Microspheres.* Berlin, Germany: Medical Radiology, Diagnostic Imaging; 2008:107–124.
23. Salem R, Thurston KG. Radioembolization with 90-yttrium microspheres: a state-of-the-art brachytherapy treatment for primary and secondary liver malignancies: part 1—technical and methodologic considerations. *J Vasc Interv Radiol.* 2006;17:1251–1278.
24. French Society of Radiation Therapy Oncology (SFRO). *Manual of External Beam Radiation Therapy Procedures.* 2007. http://www.sfro.org/sfro_pro/media/pdf/guide_procedure_radiotherapie_2007.pdf. Accessed January 29, 2014.
25. Kao YH, Tan AEH, Burgmans MC, et al. Image-guided personalized predictive dosimetry by artery-specific SPECT/CT partition modeling for safe and effective ^{90}Y radioembolization. *J Nucl Med.* 2012;53:559–566.
26. Flamen P, Vanderlinden B, Delatte P, et al. Multimodality imaging can predict the metabolic response of unresectable colorectal liver metastases to radioembolization therapy with yttrium-90 labeled resin microspheres. *Phys Med Biol.* 2008;53:6591–6603.